NANO LETTERS

2008
Vol. 8, No. 8
2188-2193

Ion Beam Doping of Silicon Nanowires

Alan Colli,*,† Andrea Fasoli,‡ Carsten Ronning,§ Simone Pisana,‡ Stefano Piscanec,‡ and Andrea C. Ferrari*,‡

Nokia Research Centre Cambridge U.K., c/o Nanoscience Centre, Cambridge CB3 0FF, U.K., Department of Engineering, University of Cambridge, Cambridge CB3 0FA, U.K., and Institute for Solid State Physics, University of Jena, Max-Wien-Platz 1, 07743 Jena, Germany

Received February 29, 2008; Revised Manuscript Received May 27, 2008

ABSTRACT

We demonstrate n- and p-type field-effect transistors based on Si nanowires (SiNWs) implanted with P and B at fluences as high as 10^{15} cm^{-2}. Contrary to what would happen in bulk Si for similar fluences, in SiNWs this only induces a limited amount of amorphization and structural disorder, as shown by electrical transport and Raman measurements. We demonstrate that a fully crystalline structure can be recovered by thermal annealing at 800 °C. For not-annealed, as-implanted NWs, we correlate the onset of amorphization with an increase of phonon confinement in the NW core. This is ion-dependent and detectable for P-implantation only. Hysteresis is observed following both P and B implantation.

The future application of silicon nanowires (SiNWs) in nanoelectronics demands a precise control over their physical properties.[1] In particular, the capability to dope them both p and n[2,3] is a key requirement if SiNWs are to be used as fundamental building blocks for complementary p/n logic gates.[4,5] The backbone of the semiconductor industry is not expected to change as novel nanocomponents are introduced.[6] Hence, the first implementation of bottom-up architectures will still rely on integration strategies based on well-developed existing technologies.[6,7]

Ion implantation is a standard doping technique in top-down semiconductor manufacturing,[8] but has been largely overlooked so far as a potential tool to dope NWs grown by bottom-up chemical methods. This technique offers precise control over total dose, depth profile, and area uniformity.[8,9] For sufficient high doses, impurity concentrations up to $10^{20}-10^{21}$ cm^{-3} (essential in many semiconductor devices)[9] can be routinely achieved. High-fluence ion bombardment, however, may induce amorphization in crystalline Si.[10] For conventional wafers, full recrystallization of the amorphous phase can be induced by annealing, since the bulk Si substrate acts as a seed for recrystallization.[10,11] For free-standing NWs, on the other hand, amorphization is in principle a major concern. If full amorphization occurs in a SiNW as a result of high-fluence implantation, it might not be possible to recover its original crystalline order.

Ion implantation in NWs has not been significantly explored so far, and the exploitation of this doping technology for bottom-up nanostructures is still very limited. Reference 12 reported implantation of an epitaxial Si overlayer grown on an intrinsic NW to form a heavily doped contact. In ref 13, portions of SiNWs lying beneath metal contacts were n-doped by ion implantation at a relatively low-fluence (4×10^{12} ions cm^{-2}), to form an n-intrinsic/n-channel. Those NWs were relatively thick (between 40 and 100 nm in diameter), but much thinner NWs are needed to further extend Moore's Law.[6]

Here we report p- and n-type field-effect transistors (FETs) based on SiNW channels 10−20 nm wide and implanted with fluences as high as 10^{15} cm^{-2}. Contrary to what would happen in bulk Si for similar fluences,[10] in SiNWs this only induces a limited amount of amorphization and structural disorder, as proven by electrical transport and Raman measurements. Furthermore, we show that a fully crystalline structure can be recovered by thermal annealing.

Our SiNWs are grown by Au-catalyzed vapor-transport as described in ref 14. The resulting NWs have a relatively thick (5−10 nm) oxide shell surrounding a crystalline Si core ~10−20 nm in diameter.[14] After synthesis, the SiNWs are mechanically transferred onto a 200 nm thick SiO_2 layer thermally grown on top of a heavily doped Si wafer, which is used as back gate (Figure 1a).[15] Ion implantation is performed on these transferred wires (Figure 1b). Source and drain contacts are then fabricated on individual NWs by e-beam lithography (Figure 1c,d) followed by a short (8 s) etching in buffered HF[16] and Ni evaporation (50 nm).

* To whom correspondence should be addressed. E-mail: alan.colli@nokia.com and acf26@eng.cam.ac.uk.
† Nokia Research Centre Cambridge U.K., University of Cambridge.
‡ Department of Engineering, University of Cambridge.
§ Universität Göttingen.

10.1021/nl080610d CCC: $40.75
Published on Web 06/25/2008

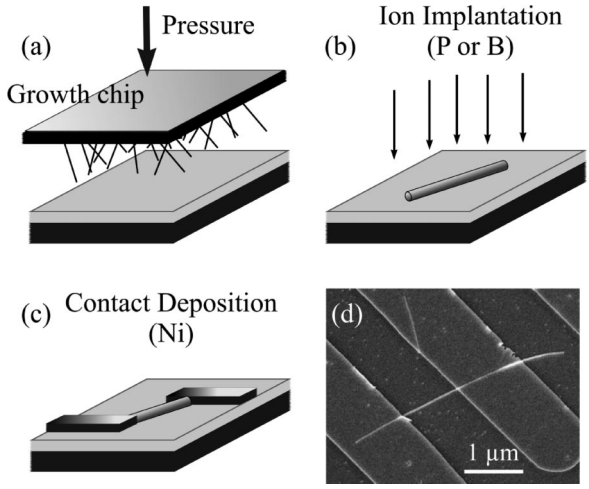

Figure 1. (a−c) Schematic illustration of NW transfer, implantation, and device fabrication. (d) Scanning electron microscope image of a typical FET device with a 1 μm long NW channel.

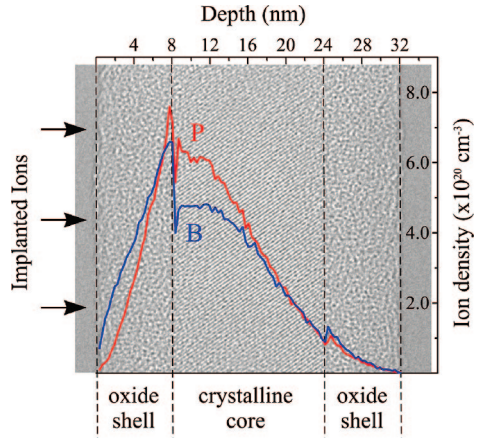

Figure 2. High-resolution TEM micrograph of a typical SiNW superimposed to the simulated implantation profiles for a corresponding $SiO_2/Si/SiO_2$ layered structure.

Given the small diameter of the wires, it is crucial to choose the correct implantation energy for each ion, to ensure the stopping range for the dopants falls within the NW core.[17] We thus simulate the implantation profiles for P and B using TRIM.[18] We model our SiNWs as a Si slab (with thickness equivalent to the NW crystalline core diameter) sandwiched between two SiO_2 slabs (with thickness equivalent to the NW oxide shell). This model neglects lateral straggle effects, i.e., implanted ions that are scattered radially outside the NW (which in bulk wafers are compensated by ions scattered from adjacent regions) and thus the predicted ion densities may be overestimated by a few percents.

Figure 2 shows a high-resolution transmission electron microscopy (HRTEM) micrograph of a typical SiNW (16 nm core and 8 nm shell) superimposed to the simulated implantation profiles for a corresponding $SiO_2/Si/SiO_2$ layered structure. Our calculations show that in order for the impurity concentration to peak in the NW core we need to use ion energies of 7 and 2.5 keV, for P and B, respectively.[19] In both cases, we also estimate that a fluence of 10^{15} cm^{-2} is necessary to have an impurity concentration above 10^{20} cm^{-3} in the NW core. Note that experimental studies on bulk Si[20] have shown that TRIM estimations are reliable in the energy range we use here for SiNWs. We therefore choose the values above as implantation parameters for all SiNWs in this study. In selected cases, we anneal the implanted SiNWs before the fabrication of the contacts. Such thermal annealing is done in a furnace for 30 min at 800 °C and in forming gas (5% H_2 in N_2) atmosphere. Transferred wires were identified with the 100× objective of a Nikon Eclipse ME600L optical microscope. Dark field imaging was used to enhance the contrast between the wires and the background. Raman spectra are measured using the 514 nm line of an Ar-ion laser coupled to a Renishaw 1000 micro-Raman spectrometer. Electrical transport is measured by means of a Cascade Microtech probe station coupled to a Keithley 4200 device analyzer.

We first investigate the electronic transport in as-implanted SiNWs. Figure 3a plots representative transfer curves (drain current versus gate voltage, I_D-V_G) for as-grown, undoped NWs. We previously showed that SiNWs synthesized by vapor-transport and contacted with Ni leads are ambipolar, with comparable ON currents for holes and electrons (ratio is usually between 2:1 and 3:1).[15] In this case, the applied gate voltage can bend the NW bands upward and downward enough for carriers (holes and electrons, respectively) to tunnel through the Schottky barriers.[14,21,22] Thus, the ambipolar behavior of our pristine SiNWs is ideal to study doping, because any effect in either direction can be detected as an ON current reduction for minority carriers. In fact, n-type (p-type) doping changes the band alignment for a metal-semiconductor junction so that the conduction (valence) band moves closer to the Fermi level,[9] facilitating the gate-induced electron (hole) tunneling through the Schottky barrier while hindering hole (electron) injection. We thus consider the evolution from ambipolar to unipolar behavior as a qualitative indicator of band-alignment and, therefore, of doping.

The hysteresis observed in Figure 3a when reversing the gate sweeping direction is generally thought to arise from charge trapping at surface states or defects in the oxide.[14,23,24] The hysteresis gap (i.e., the threshold voltage shift upon reversing the sweep) for as-grown NWs is roughly 10−15 V (Figure 3a). Figure 3b,c shows transfer curves taken at different drain-source voltages (V_{DS}) for P- and B-implanted SiNWs, respectively. These wires are not further treated after implantation, except for the processing needed for device fabrication. Yet, doping is achieved in both cases, as seen from the unipolar behavior in Figure 3b,c. As expected, P-implantation results in n-type FETs, while a p-type response is measured following B-implantation. Note that the hysteresis is strongly enhanced for both P- and B-implanted samples, when compared with pristine SiNWs, with hysteresis gaps up to 60 V (Figure 3b,c).

Ion-implantation in semiconductors is known to cause defects and deep states, leading eventually, for high fluences, to amorphization.[10,11] Defects introduced in the crystal are scattering centers and must be annealed out to recover a good crystalline quality and fully activate the implanted dopants.[10,11] It is thus not surprising that our doped SiNWs

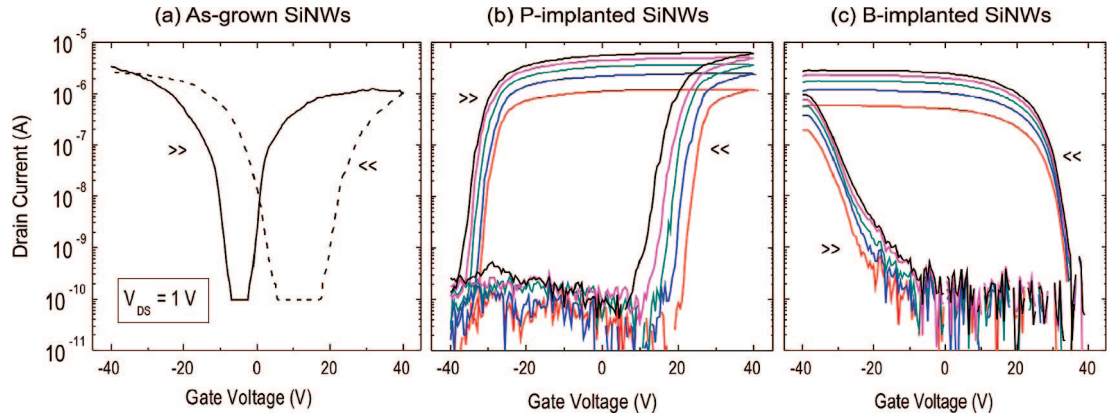

Figure 3. Transfer curves for (a) as-grown SiNWs ($V_{DS} = 1$ V), (b) P-implanted SiNWs (red to black: $V_{DS} = 0.2$, 0.4, 0.6, 0.8, 1 V) and (c) B-implanted SiNWs (legend as for panel b). Consecutive gate sweeps for increasing (≫) and decreasing (≪) V_G are presented. The FET ON state is found for positive V_G in panel b and for negative V_G in panel c, consistently with the implanted impurities. Large hysteresis gaps up to 60 V are measured for implanted NWs.

show a larger hysteresis, since we expect them to have many unpassivated states, prone to charge trapping. Yet, it is noteworthy that parameters such as ON currents and subthreshold slopes are closely comparable to those of as-grown NW transistors. This suggests that the structural damage induced in the crystal by high-fluence ion-bombardment is relatively limited and does not cause a significant degradation of the NW electrical properties.

A remarkable difference with respect to as-implanted NWs in Figure 3b,c is seen in the electrical response of doped SiNWs annealed after implantation. Figure 4a,b shows transfer curves for annealed SiNWs, P and B doped, respectively. Again, we sweep the gate voltage in both directions to monitor hysteresis. For annealed samples, the hysteresis gap is far lower than for not-annealed ones (Figure 3b,c). Essentially, the original hysteresis of as-grown, undoped NWs (Figure 3a) is restored (10−15 V or lower).

The activation of the implanted P and B impurities needs some consideration. The binding energy of the donor/acceptor state is 0.045 eV.[9] If all the implanted ions were incorporated as substitutional impurities, the free carrier concentration at room temperature would be well above 10^{19} cm^{-3} [by scaling the values 4–6 × 10^{20} cm^{-3} in Figure 2 by the Boltzmann factor $\exp(-0.045\ eV/K_BT) = 0.165$]. In this regime, the conduction or valence band (in the case of P or B, respectively) would almost coincide with the Fermi level,[9] and its pinning close to the interface would be so steep to almost behave like an ohmic contact (thus resulting in unipolar FETs). Yet, we note that the transfer curves in Figure 4a,b are slightly ambipolar. They are a signature of n- and p-type SiNWs, since the ON current for minority carriers (holes in (a), electrons in (b)) is suppressed by about 2 orders of magnitude, compared with a typical intrinsic-NW device (Figure 3a). However, such weak ambipolar behavior indicates that the concentration of majority carriers is lower than that predicted in the full-activation limit.

It was suggested that dopant impurities in semiconductor NWs tend to segregate at the NW surface.[25,26] In this case, a large proportion of dopants would therefore be trapped and electrically neutralized at surface states, thus reducing the

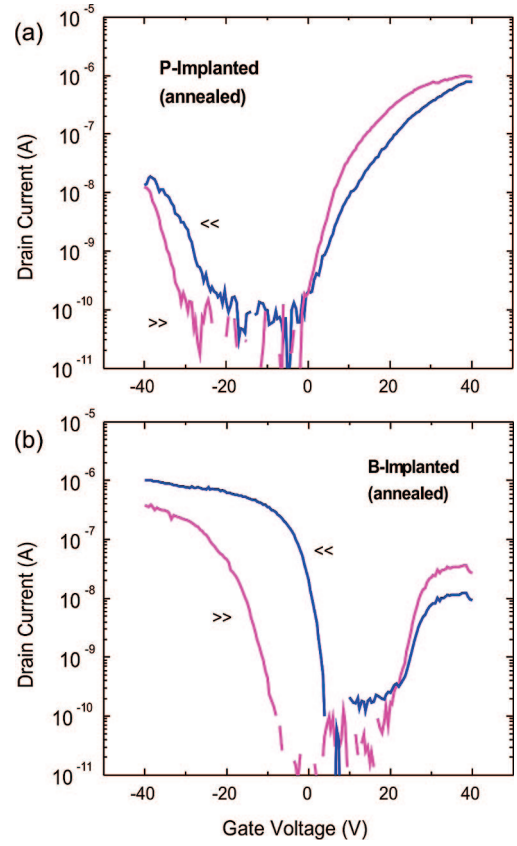

Figure 4. Consecutive transfer curves for increasing (≫) and decreasing (≪) gate voltage for (a) P-doped and (b) B-doped SiNWs annealed at 800 °C after implantation ($V_{DS} = 1$ V). All curves show a weak ambipolar behavior. In both cases, hysteresis gaps are recovered to values similar to those in Figure 3a for as-grown SiNWs.

density of free carriers. We believe that annealing thin NWs at high temperature may enhance diffusion of impurities in the crystal, resulting in dopant migration and segregation at the NW surface. This may lead to a *lower* doping concentration in the NW core with respect to not-annealed SiNWs, where unipolar behavior is observed (Figure 3b,c). However, the stronger hysteresis in Figure 3b,c should also be taken into account when comparing annealed and not-annealed

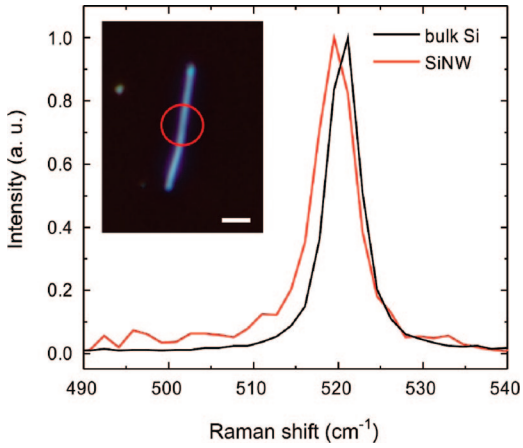

Figure 5. Raman spectra of bulk Si (black) and as-grown SiNWs (red). The inset shows a dark-field optical microscope image of an individual SiNW. The red circle indicates the laser spot size. Scalebar is 1 μm.

SiNWs, as more trap states can screen more efficiently the applied gate voltage. Improving the annealing procedure (for example by using rapid-thermal-annealing) could minimize diffusion, while ensuring good activation efficiency.

Raman spectroscopy is one of the preferred tools for the nondestructive characterization of SiNWs, being very sensitive to disorder and size.[27] To further investigate the structural evolution of SiNWs upon implantation and annealing, we measure the Raman spectra from individual SiNWs at various processing stages. For these experiments, as-grown SiNWs are initially transferred to a quartz substrate (to avoid any Raman contribution from the silicon substrate) and then implanted and annealed in the same conditions used for the devices discussed above.

We first compare in Figure 5 the Raman spectrum of a representative as-grown SiNW with that of bulk Si. For NWs (red curve), the first order Si peak[28] is downshifted ($\sim$1 cm^{-1}) and asymmetrically broadened compared to bulk Si. We have previously shown that SiNWs are particularly sensitive to the laser power.[27] Even moderate powers, which do not give any effect in bulk Si, can result in very significant local heating of NWs. Several previous claims of detection of phonon confinement in NWs[29] were in fact a result of laser induced heating of the SiNWs.[27] To properly interpret our results, we must first ensure that no laser-induced heating is present. We have thus monitored the anti-Stokes/Stokes intensity ratio (which depends on the local temperature via the exponential factor $\exp(K_B T/\hbar\omega_0)$)[30] in the power range used for our experiments. We found this to be constant and consistent with the room temperature ratio measured on bulk Si. Hence, we can exclude any significant anharmonic effects and safely assign the features observed in Figure 5 to quantum confinement.

We can then derive an estimation of the diameter of the crystalline core for each SiNW we measure. Due to the Heisenberg's uncertainty principle, the fundamental $q \sim 0$ Raman selection rule is relaxed for a finite-size domain, allowing the participation of phonons away from the center of the Brillouin zone.[31,32] The uncertainty on the phonon

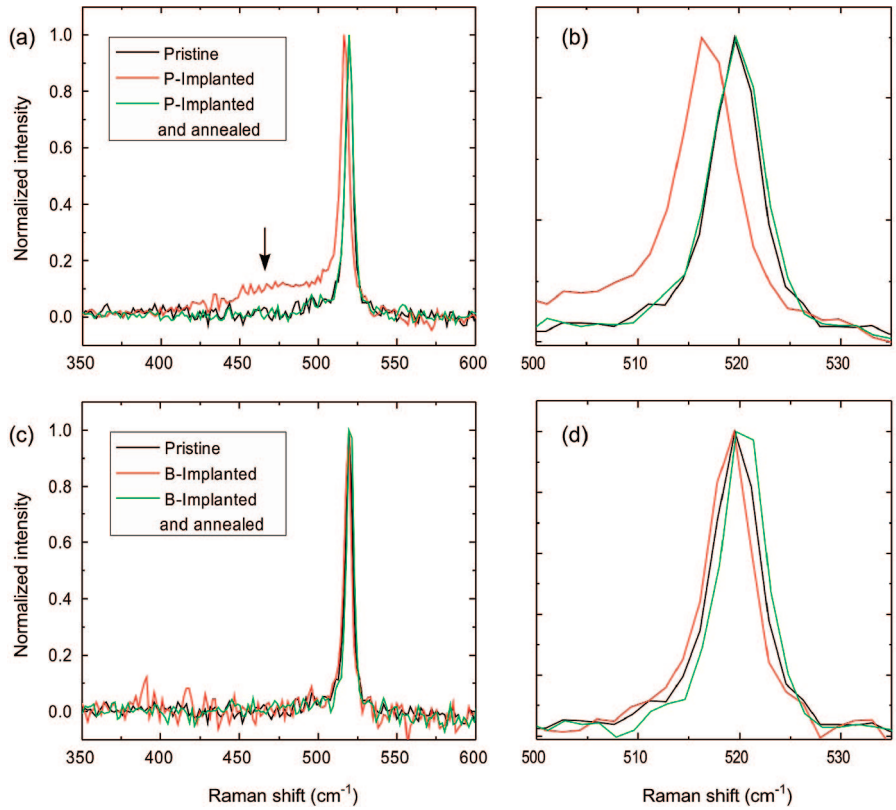

Figure 6. Raman spectra of as-grown (black), implanted (red) and annealed (green) SiNWs for (a,b) P-implantation and (c,d) B-implantation. In panels b and d, the region around 520 cm^{-1} is magnified, highlighting the shift and broadening that occurs to the Si peak for P-implantation and the line-shape recovery upon annealing at 800 °C. Negligible peak shifts are seen for B-implantation.

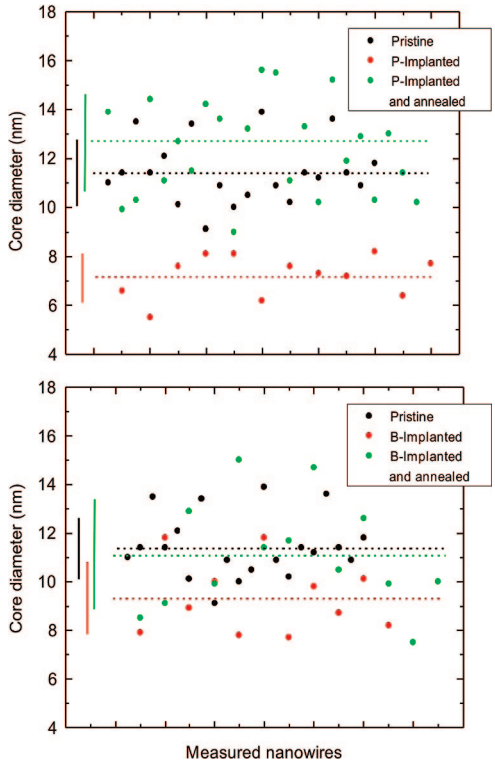

Figure 7. Effective core diameter distribution of as-grown (black), implanted (red) and annealed (green) SiNWs for (a) P-implantation and (b) B-implantation. Average diameters (horizontal dotted lines) and standard deviations (vertical lines close to left axis) are emphasized.

wave-vector goes roughly as $\Delta q \sim 1/d$, where d is the measure of the confined dimension (in our case the NW core diameter). The effects of phonon confinement on the shape of the Raman spectra of SiNWs can be described by adapting the model proposed by Richter, Campbell, and Fauchet (RCF model),[31,32] as we have done in reference 27:

$$I(\omega) = \int \frac{|C(q)|^2}{[\omega - \omega(q)]^2 + (\Gamma_0/2)^2} d^2q \qquad (1)$$

where C(q) are the Fourier coefficients of the confinement function, Γ_0 and $\omega(q)$ are, respectively, the natural phonon line-width and the phonon dispersion of the center zone optical phonon of silicon. By fitting the SiNW spectrum in Figure 5 with eq 1, we get a diameter of 12 nm, consistent with the typical crystalline core of a pristine SiNW, as determined by TEM (Figure 2). Statistics over tens of individual, pristine SiNWs further confirm an average value for the core diameter of ~12 nm.

Figure 6a compares the Raman spectra for as-grown NWs (black), NWs implanted with P (red), and postimplantation annealed at 800 °C (green). The same comparison for B-implanted NWs is shown in Figure 6c. In all cases, the dominant Raman contribution comes from the first order crystalline Si (c-Si) peak. We note however that, for P-implanted, not-annealed SiNWs (red curve in Figure 6a), an additional broad peak arises at about 480 cm^{-1} (black arrow), which indicates the presence of an amorphous Si (a-Si) phase.[33] Upon annealing, the a-Si contribution disappears (green curve in Figure 6a) and the SiNW spectrum closely resembles that of the pristine unimplanted SiNW. On the other hand, no amorphous peak is found in Figure 6c for B-implantation. A similar trend is observed when considering the line-shape evolution of the Raman spectra (Figure 6b,d). Compared to pristine SiNWs, P-implanted and not-annealed SiNWs have a further downshift and asymmetric broadening of the c-Si peak. Their line-shape again reverts to the as-grown condition for annealed NWs. For B-implanted SiNWs (Figure 6c), we do not detect appreciable changes within our spectral resolution.

These combined observations are consistent with an enhancement of phonon confinement concomitant to a partial amorphization of the NW core. To better quantify this, we consider large statistics of Raman spectra (up to 20 different NWs measured individually per processing stage) and extract (as explained above) for each NW an effective core diameter, Figure 7. This is the size over which the phonons are confined, but clearly does not imply a reduction of the average overall diameter of the NWs. The horizontal lines in Figure 7 represent the average phonon-confinement size, while the vertical lines are the standard deviation. Figure 7a shows that P-implantation in our SiNWs causes a reduction of the crystalline core diameter of about 4 nm, which is later reversed by the annealing.

Reference 34 attributed a down-shift and symmetric broadening of the Raman peak, following ion implantation in bulk Si, to amorphization-related strain. In our case however, the broadening for P-implanted SiNWs (Figure 6c, red spectrum) is clearly asymmetric, thus ruling out this possibility. Further, it has been suggested that free carriers might interfere with the Si phonon line to give rise to an asymmetric Fano line-shape.[35] Electrons would give a low frequency asymmetry and a downshift of the Raman peak, while holes a high-frequency asymmetry and an upshift.[35] In heavily p- and n-doped Si, this can affect the spectrum shape dramatically.[36,37] Here, however, we can disregard this effect for the following reason. Even assuming a case of heavily n-doped Si (10^{20} donors/cm^3), the resulting peak downshift would be less than 0.5 cm^{-1} (see ref 37, Figure 4). On the other hand, the Fano effect was found to be stronger for p-type Si and was observed for B doping concentrations as low as 4×10^{18} cm^{-3}.[38] Hence, if this were responsible for the line-shape evolution in our case, we should observe a high-frequency asymmetry for B-implanted NWs as the dominant effect, rather than a low-frequency asymmetry for P-implanted NWs only.

Figures 6, 7 show that P-implantation at 10^{15} ions/cm^2 results in a partial amorphization of our SiNWs, whereas for B-implantation at identical fluence this effect is negligible. This is consistent with what previously reported in ref 10 for implantation in bulk Si, where, for fixed fluence, the amorphization was found to be proportional to the ion mass. We stress, however, that a fluence of 10^{15} ions/cm^2 is nominally well above the full-amorphization threshold for P-implantation at room temperature (2×10^{14} ions/cm^2) in bulk Si.[10] Still, the a-Si contribution to the Raman spectrum in Figure 6a (red curve) is merely a shoulder of the dominant c-Si peak, indicating that most of the SiNW core preserves

its crystalline nature upon implantation. To explain this, we speculate that dynamic annealing (removal of defects induced by the ion beam as a consequence of the energy delivered by the ions themselves[39]) may play an important role in SiNWs. The authors in ref 40 observed that dynamic annealing is enhanced for GaN NWs during Ga^+ implantation. Such a result could be generalized, since it may be triggered preferentially by morphology-dependent properties (high diffusivity of mobile point defects[40] and limited thermal conductivity of thin NWs[41]), rather than by the particular stoichiometry of the nanostructures.

Finally, by combining the Raman data with the transport measurements in Figure 3b,c, we infer that the hysteresis effect observed for our devices cannot be associated with amorphization of the SiNW channel. In fact, the large increase of the hysteresis gap for P- and B-doped NWs (Figure 3) shows no dependence on the implanted ions. We therefore conclude that defects and traps created by the implantation process are mainly localized within the oxide shell or at the core/shell interface. This is a critical result, as it shows that SiNW-based devices can be assembled and doped by ion implantation even on substrates that would not allow a subsequent high-temperature annealing treatment (e.g., plastic). The defected oxide shell responsible for hysteresis could then be etched away prior to embedding the NW cores (whose performance is not substantially affected by a limited degree of amorphization, Figure 3) into a suitable insulating matrix for better surface passivation.[13]

In summary, we demonstrated n- and p-type field-effect transistors (FETs) based on SiNWs implanted with P and B at fluences as high as 10^{15} cm^{-2}. Raman spectroscopy and electrical measurements show that the limited amount of amorphization and structural disorder due to ion-bombardment can be recovered by annealing at 800 °C. For not-annealed NWs, we correlated SiNW amorphization with a down-shift and an asymmetric broadening of the c-Si Raman peak, consistent with an increase of phonon confinement in the NW core. While amorphization is ion-dependent and detectable for P-implantation only, the significant hysteresis observed for implanted-SiNW devices is independent of the particular atom species used as dopant.

Acknowledgment. We thank T. Butler for assistance with e-beam lithography. A.F. acknowledges funding from Pembroke College, EPSRC, Cambridge European Trust, and the Ministry of Information and Communication, Republic of Korea (Project No. A1100-0602-0101). A.C.F. acknowledges funding from The Royal Society, and The Leverhulme Trust.

References

(1) Li, Y.; Qian, F.; Xiang, J.; Lieber, C. M. *Mater. Today* **2006**, *9*, 18.
(2) Cui, Y.; Duan, X.; Hu, J.; Lieber, C. M. *J. Phys. Chem. B* **2000**, *104*, 5213.
(3) Zheng, G.; Lu, W.; Jin, S.; Lieber, C. M. *Adv. Mater.* **2004**, *16*, 1890.
(4) Wang, D.; Sheriff, B. A.; Heath, J. R. *Small* **2006**, *2*, 1153.
(5) Huang, Y.; Duan, X.; Cui, Y.; Lauhon, L. J.; Kim, K.-H.; Lieber, C. M. *Science* **2001**, *294*, 1313.
(6) Barrett, C. R. *MRS Bull.* **2006**, *31*, 906.
(7) Colli, A.; Fasoli, A.; Pisana, S.; Fu, Y.; Beecher, P.; Milne, W. I.; Ferrari, A. C. *Nano Lett.* **2008**, *8*, 1358.
(8) *Handbook of ion implantation*; Ziegler, J. F., Ed.; North-Holland: Amsterdam, 1992.
(9) Sze, S. M. *Physics of Semiconductor Devices*; Wiley: New York, 1981.
(10) Pelaz, L; Marqués, L. A.; Barbolla, J. *J. Appl. Phys.* **2004**, *96*, 5947.
(11) Picfnar, K. A. Ion Implantation in Silicon-Physics, Processing and Microelectronic Devices. In *Applied Solid State Science*; Wolfe, R., Ed.; Academic: New York, 1975; Vol. 5.
(12) Cohen, G. M.; Rooks, M. J.; Chu, J. O.; Laux, S. E.; Solomon, P. M.; Ott, J. A.; Miller, R. J.; Haensch, W. *Appl. Phys. Lett.* **2007**, *90*, 233110.
(13) Hayden, O.; Bjork, M. T.; Schmid, H.; Riel, H.; Drechsler, U.; Karg, S. F.; Lortscher, E.; Riess, W. *Small* **2007**, *3*, 230.
(14) Colli, A.; Fasoli, A.; Beecher, P.; Servati, P.; Pisana, S.; Fu, Y.; Flewitt, A. J.; Milne, W. I.; Robertson, J.; Ducati, C.; De Franceschi, S.; Hofmann, S.; Ferrari, A. C. *J. Appl. Phys.* **2007**, *102*, 034302.
(15) Colli, A.; Pisana, S.; Fasoli, A.; Robertson, J.; Ferrari, A. C. *Phys. Status Solidi B* **2007**, *244*, 4161.
(16) The etching in buffered HF is necessary to expose the crystalline NW core beneath the contacts. For thermal SiO_2, we measured an etch rate of ~100nm/min. An etching time of 8 s is thus long enough to strip off a 13 nm thick oxide shell. Accordingly, increasing the etch time did not result in any improvement in the quality of the contacts.
(17) Ziegler, J. F.; Biersack, J. P.; Littmark, U. *The Stopping and Ranges of Ions in Solids*; Pergamon: New York, 1985.
(18) *The stopping range of ions in matter* at www.srim.org (accessed June 2008).
(19) Note that simulations in Figure 2 consider a trajectory thorough the NW centre. Ions impinging close to the NW edge would travel through a thinner portion of material. The slight left-shift for the peaks in Figure 2 qualitatively compensates for this effect.
(20) Collart, E. J. H.; Weemers, K.; Cowern, N. E. B.; Politiek, J.; Bancken, P. H. L.; van Berkum, J. G. M.; Gravesteijn, D. J. *Nucl. Instrum. Methods Phys. Res., Sect. B* **1998**, *139*, 98.
(21) Koo, S.-M.; Li, Q.; Edelstein, M. D.; Richter, C. A.; Vogel, E. M. *Nano Lett.* **2005**, *5*, 2519.
(22) Ahn, Y.; Dunning, J.; Park, J. *Nano Lett.* **2005**, *5*, 1367.
(23) Byon, K.; Tham, D.; Fischer, J. E.; Johnson, A. T. *Appl. Phys. Lett.* **2005**, *87*, 193104.
(24) Weber, W. M.; Geelhaar, L.; Graham, A. P.; Unger, E.; Duesberg, G. S.; Liebau, M.; Pamler, W.; Cheze, C.; Riechert, H.; Lugli, P.; Kreupl, F. *Nano Lett.* **2006**, *6*, 2660.
(25) Fernandez-Serra, M. V; Adessi, Ch.; Blase, X. *Phys. Rev. Lett.* **2006**, *96*, 166805.
(26) Peelaers, H.; Partoens, B.; Peeters, F. M. *Appl. Phys. Lett.* **2007**, *90*, 263103.
(27) Piscanec, S.; Cantoro, M.; Ferrari, A. C.; Zapien, A.; Lifshitz, Y.; Lee, S. T.; Hofmann, S.; Robertson, J. *Phys. Rev. B* **2003**, *68*, 241312.
(28) Temple, P. A.; Hathaway, C. E. *Phys. Rev. B* **1973**, *7*, 3685.
(29) (a) Li, B. B.; Yu, D. P.; Zhang, S. L. *Phys. Rev. B* **1999**, *59*, 1645. (b) Wang, R. P.; Zhou, G. W.; Liu, Y. L.; Pan, S. H.; Zhang, H. Z.; Yu, D. P.; Zhang, Z. *Phys. Rev. B* **2000**, *61*, 16827. (c) Zhang, S. L.; Ding, W.; Yan, Y.; Qu, J.; Li, B.; Li, L. Y.; Yue, K. T.; Yu, D. P. *Appl. Phys. Lett.* **2002**, *81*, 4446. d) Eklund, P. C. *Proceedings of the XVIIIth International Conference on Raman Spectroscopy*; Wiley: New York, 2002.
(30) Bruesch, P. *Phonons: Theory and Experiments I - Lattice Dynamics and Models of Interatomic Forces*; Springer: Berlin, 1982.
(31) Richter, H.; Wang, Z. P.; Ley, L. *Solid State Commun.* **1981**, *39*, 625.
(32) Campbell, I. H.; Fauchet, P. M. *Solid State Commun.* **1986**, *58*, 739.
(33) Bermejo, D.; Cardona, M. *J. Non-Cryst. Solids* **1979**, *32*, 405.
(34) Motooka, T.; Holland, O. W. *Appl. Phys. Lett.* **1991**, *58*, 2360.
(35) Gupta, R.; Xiong, Q.; Adu, C. K.; Kim, U. J.; Eklund, P. C. *Nano Lett.* **2003**, *3*, 627.
(36) Cerdeira, F.; Fjeldly, T. A.; Cardona, M. *Phys. Rev. B* **1973**, *8*, 4734.
(37) Chandrasekhar, M.; Renucci, J. B.; Cardona, M. *Phys. Rev. B* **1978**, *17*, 1628.
(38) Magidson, V.; Beserman, R. *Phys. Rev. B* **2002**, *66*, 195206.
(39) Prussin, S.; Margolese, D. I.; Tauber, N. C. *J. Appl. Phys.* **1983**, *54*, 2316.
(40) Dhara, S.; Datta, A.; Wu, C. T.; Lan, Z. H.; Chen, K. H.; Wang, Y. L.; Chen, L. C.; Hsu, C. W.; Lin, H. M.; Chen, C. C. *Appl. Phys. Lett.* **2003**, *82*, 451.
(41) Li, D.; Wu, Y.; Kim, P.; Shi, L.; Yang, P.; Majumdar, A. *Appl. Phys. Lett.* **2003**, *83*, 2934.

NL080610D